Evaluation of a 7-DoFs Robotic Manipulator as haptic interface during planar reaching tasks

Alessia Noccaro[1,2], Silvia Buscaglione[2], Mattia Pinardi[2], Giovanni Di Pino[2] and Domenico Formica[1,2]

***Abstract*— In this work, we evaluated the suitability of using a 7 degrees of freedom robotic manipulator as a planar haptic interface for studies in motor neuroscience. In particular, we assessed to what extent it can measure human movement and forces without applying undesired perturbations. To this aim, we evaluated the amount of perturbation exerted by the robot during planar reaching movements when controlled to be as transparent as possible in the 2D task space, through an impedance control. Two planar specular configurations of the robot were tested, namely G1 and G2, which differ in the position of the "elbow joint" in the workspace. For both configurations, we estimated the inertial ellipsoids and simulated the forces for human-like forward movements. Performance was then experimentally assessed on 8 healthy participants, in 15 different positions in the workspace. The average handpath perturbation decreased and settled to 6 mm after 2 minutes of interaction. Interaction forces resulted specular for G1 and G2, with mean values below 5 N. Overall, the robotic manipulator resulted suitable for studies on planar reaching movements in both configurations, with a preference for the G1 configuration due to its symmetrical distribution of trajectory deviations, which anyway remain well below 1 cm for movements of 15 cm.**

I. Introduction

The use of robots to analyze or assist human motion is a major and extensive topic both in research and rehabilitation, particularly when concerning the upper limbs.

In motor neuroscience, robots have been used as a means to analyze human movement while precisely and deliberately perturbing it by providing, for instance, haptic disturbances, in order to investigate motor adaptation to environmental dynamics and uncover the rules that govern human motor control. Indeed, robotic manipulators were used to apply stable and unstable force fields during human movements, while measuring displacements and forces, in order to evaluate the formation of motor memory [1]–[4].

In particular, the study of reaching movements perturbed through planar robots has proven that humans build an internal model of the perturbation field, which they use to compensate for external forces during movements [5], [6]. Similarly, the use of robotic devices to measure forces exerted by the human arm during planar movement in unstable fields, proved that the Central Nervous System selectively controls the endpoint impedance to adapt to the environment [7], [8].

Moreover, robotic devices have been also employed in stroke rehabilitation for delivering enhanced sensorimotor training in the case of a paralyzed upper limb [9], [10], proving how rehabilitation conducted with a task-specific robot resulted in a significant improvement for patients with moderate disability [11].

Most of the robots employed in these studies on upper limbs, both for rehabilitation or research purposes, are planar devices [12], [13]. The reason is twofold: i) a planar workspace allows for a simpler mechanical and control design of the robot; ii) planar movements allow to simplify the model of the human arm and easily define additional force fields as well as simple exercises when dealing with rehabilitation tasks [14].

Besides their planar workspace, an important feature of these planar devices is the low inertia at the end-effector, achieved through hardware strategies (e.g. motors located at the robot base), sometimes combined with software strategies (e.g. active control of the motors to compensate for the robot dynamics) [15], [16]. This feature, which prevents unintended interference during the measures of human movements, is crucial for neuroscience studies which aim at inferring what regulates human motor control by applying carefully controlled perturbations [17].

Here, we aim to investigate if general-purpose collaborative robotic manipulators (COBOTS), which are designed for human-robot interactive tasks with a wide range of possible applications (i.e. not specifically designed for their use as haptic interface), could be employed in motor neuroscience experiments without inadvertently affecting the task outcome. Thus, we evaluated the feasibility of using a 7 Degrees of Freedom (DoFs) robotic manipulator, i.e. Panda Robot, as a transparent haptic interface in motor control and adaptation studies. In particular, we assessed the amount of perturbation, quantified by the deviations from the straight path, and the amount of interaction forces provided by the robot on the human arm during planar reaching movements across the workspace.

To test the robot's suitability for such planar tasks, we constrained its motions to a 2D workspace, using a selective impedance set to zero in the 2D task space and to high values for the other directions (II-B). We tested two alternative robot configurations compatible with the requirements of the tasks, which differ in the position of the "elbow joint" in the space (see II-A and fig. 1), to assess which one is affecting human performance less.

This work was supported by the European Commission under H2020 grant CONBOTS (ICT 871803) and under the "NIMA: Non-invasive Interface for Movement Augmentation" project (H2020-FETOPEN-2018-2020, ID: 899626).

[1]Neurorobotics Lab, Newcastle University, Newcastle upon Tyne, United Kingdom

[2]NEXT: Neurophysiology and Neuroengineering of Human-Technology Interaction Research Unit, Università Campus Bio-Medico di Roma, Italy.

Email: alessia.noccaro@newcastle.ac.uk

To assess the theoretical impact of robot dynamics, we first simulated the inertia ellipses of the robot in different configurations across the workspace (II-C and II-D). Then, we tested it in a reaching task on eight healthy volunteers, measuring the movement deviations and the interaction forces (II-E and II-F). The robot was controlled using an impedance control, which included the compensation for known robot dynamics, in terms of gravity, Coriolis and centrifugal contribution and joint viscous friction.

This study opens the way to the use of general-purpose collaborative manipulators to conduct human experiments in motor neuroscience, which will permit the implementation of a wider range of possible tasks and with a larger workspace with respect to specific haptic interfaces. In fact, the higher number of DoFs of a robotic manipulator rather than planar robots might allow the extension of motor control studies to more complex tasks, facilitating the translation of knowledge to real-life applications, such as in less structured rehabilitation scenarios.

II. Materials and Methods

To assess the suitability of a 7-DoFs manipulator (Panda Robot by Franka Emika GmbH) as a transparent haptic interface, we evaluated the amount of interference provided by the robot on human motion during a reaching task performed in the horizontal plane.

Although the ideal scenario would be the robot providing null forces, we expect a non-null force field due mainly to robot inertia. In fact, despite the active control implemented for compensating the effect of gravity, Coriolis and joint viscous friction, the kinematic chain, including links, motors and sensors, leads to non-negligible inertia when the robot is manually moved.

This inertia contribution was first estimated, in terms of 2D inertia ellipses in the task space and inertial forces, through the simulation of the robot model in the different configurations across the workspace. Then, we conducted an experiment on healthy volunteers to assess how much the actual dynamic of the robot affects natural movements in real conditions during human-robot interaction. The evaluated workspace was defined by the positions reachable on average by the human hand during planar movements, with the hand moving at the same height as the shoulder (see fig. 2).

A. Planar Configuration

The robot was arranged into a planar configuration, i.e. with the end-effector moving only in the horizontal plane, by moving the elbow joint and the end-effector to the same height as the robot base (note that the first rigid link is considered here as though part of the base). This planar configuration allows to implement planar motions by moving only 2 robots joints, and can be set up either with a clockwise or counterclockwise rotation of the elbow joint, i.e. leading to two mirrored configurations named *G1* and *G2*, as depicted in figure 1. In the present work, we evaluated both configurations in terms of perturbation provided to the movement of participants during reaching tasks.

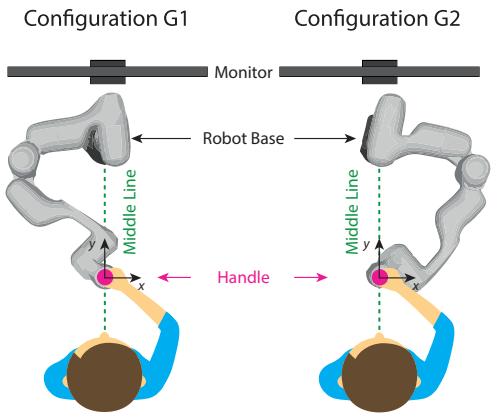

Fig. 1. Schematic representation of the robot configurations. The robot is positioned in a planar configuration with the elbow and end-effector on the same horizontal plane as the robot base. The green dashed line represents the middle line (y-axis) of the workspace. In configuration G1 the robot's elbow is located on the left side of the workspace, whereas in configuration G2 is located on the right side.

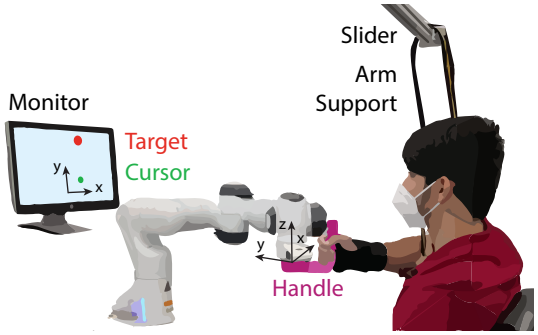

Fig. 2. Experimental setup in configuration G2. The participant is seated in front of the robot with the head aligned with the robot base and the monitor and holds the ergonomic handle fixed on the end-effector. The participant's hand, elbow and shoulder lay onto the same horizontal plane (xy). The arm's weight is compensated through a strap fixed to a slider.

B. Robot Control

During the task, the robot was controlled through an impedance control (by means of a torque control), with a high impedance along all the directions except the ones involved in the task, i.e., the translations on the horizontal plane, where the robot presents null impedance, making the robot as transparent as possible in the task space. Overall the commanded torque τ resulted composed of three contributions:

$$\tau = \tau_s + \tau_w + \tau_n \,. \tag{1}$$

The first torque vector was calculated as follows:

$$\tau_s = J^T[Ke - D(J\dot{q})] + C + g \,, \tag{2}$$

where J is the 6x7 Jacobian matrix, $e = p_d - p$ is the error vector, with p the 6x1 vector of the actual end-effector pose with respect to the base frame and p_d is the desired pose, which is set to be equal to the starting pose. K and D are the 6x6 stiffness and damping matrices expressed in the Cartesian space, and C and g represent the Coriolis and centrifugal, and gravity generalized forces in the joint space,

respectively. In order to constraint movements along the horizontal plane, the impedance was selectively set along space directions. Stiffness and damping values were chosen to be very high along the z-axis for translations and all three axes for rotations, while zero along the 2 translations DoFs of the task (x and y), with $K = diag(0, 0, K_z, K_r, K_r, K_r); D = diag(0, 0, D_z, D_r, D_r, D_r)$; $K_z = 2500N/m$, $D_z = \sqrt{K_z}\ Ns/m$, $K_r = 60\ Nm/rad$ and $D_r = \sqrt{K_r}\ Nms/rad$. All impedance values are defined with respect to the robot base reference frame.

We also compensated for the joint viscous friction by adding the contribution $\tau_w = cW\dot{q}$ to the joint torques. W is a 7x7 diagonal matrix whose diagonal values were derived from a linear regression between the torques and joint velocities data acquired while manually moving the robot in *Zero-Torque* control. The effect of τ_w is to add a positive torque that increases with the joint velocity, in order to compensate for joint viscous friction. In order to avoid stability issues we limited this compensation to 50% of the estimated torques, by multiplying the estimated friction torques $W\dot{q}$ by the coefficient $c = 0.5$.

In order to manage the redundant DoF of the robot, an additional torque projected into the null space was included in the control law [18]:

$$\tau_n = (I - J^T J^{\dagger T})[k_n(q_{dn} - q) - d_n\dot{q}]\,, \qquad (3)$$

where q_{dn} is the desired joint position vector and it is equal to the initial configuration; q is the current joint position vector; $k_n = 20\ Nm/rad$; $d_n = \sqrt{k_n}\ Nms/rad$; I is a 7x7 identity matrix and $J^\dagger = J^T(JJ^T)^{-1}$. The null space contribution allowed to avoid that the joint angles, not involved in the task movements, drift when subjects perform repetitive movements [19].

C. Reaching Task

Participants were asked to reach virtual targets by moving a virtual cursor via the robotic handle. Robot and arm movements were constrained in the horizontal (xy) plane.

In order to span approximately the whole workspace reachable with the human arm, 15 positions centred with the robot base reference frame, and evenly spaced 2.5 cm apart, were identified on the horizontal (x) axis. For each position, participants were asked to reach the corresponding target (15 cm distant) by moving the handle forward (along the y-axis) on a straight line, as accurately as possible.

Each trial had a 2 seconds timeout, after which the target position disappeared and the new starting position was displayed. Trials were separated by a 2.5 seconds break in which the robot moved to the next starting position, always maintaining the planar configuration and the same end-effector orientation with respect to the robot base.

D. Simulation of Inertial contribution

Considering the robot control in (1), the main residual element that needs to be compensated to move the robot is its inertia in the 2D task space. Thus, we estimated the inertial forces required to perform planar forward reaching movements, with the two robot configurations. We simulated different robot movements and postures along the trajectory of interest, by means of the open-source 3D robotics simulator Gazebo and the robotics middleware suite Robot Operating System (ROS).

The same 15 positions considered in the task were evaluated for the simulations. For each position, we estimated a 15 cm movement along the y-axis, performed in 1 second.

We simulated a human-like movement along the y-axis through a minimum jerk trajectory, in which the position p is calculated by a fifth-order polynomial as a function of time. For each trajectory, we estimated the inertial ellipsoids and inertial forces F at 5 intermediate points (8, 30, 50, 70 and 92 % of the total path) as follows:

$$F = \Lambda\ddot{p}\,, \qquad with\ \Lambda = J^{-T}BJ^{-1}\,, \qquad (4)$$

where B is the 7x7 kinetic energy matrix in the joint space, estimated through the robot model, and Λ is the 6x6 kinetic energy matrix in the operational space. The generalized inertia ellipses on the horizontal plane were evaluated considering Λ_2, which represents the sub-matrix of Λ composed of its first two rows and columns. The principal axes of the ellipse are aligned with Λ_2 eigenvectors $\lambda(\Lambda_2)$ and their lengths are $1/\sqrt{\lambda(\Lambda_2)}$ [16]. Similarly, only the x and y contributions of the inertial forces were considered in the analysis.

E. Experimental Protocol

Eight healthy participants (32.33 $\pm$ 6.57 years old, four female) took part in the study, after having signed written informed consent. Experimental procedures were approved by the Ethics Committee of Università Campus Bio-Medico di Roma (HUROB protocol) and carried out according to the Declaration of Helsinki. Participants were all right-handed, as assessed through the Oldfield test [20].

Each participant performed two experimental sessions, two hours apart, each one with one of the robot configurations. Four of them (two males and two females) started with configuration *G1* and the others with configuration *G2*.

Within each session, participants performed three task repetitions, each composed of 30 trials (2 per position) in random order. One repetition lasted roughly 2 minutes, including intermediate breaks. The number of repetitions allowed participants to familiarize with the experimental setup, but most importantly to potentially adapt to the force field provided by the robot.

F. Experimental Setup

A 7-DoFs Panda robot (by Franka Emika GmbH) was employed and a custom ergonomic handle was 3D-printed and fixed to the robot end-effector. Participants sat on a chair, in front of the robotic manipulator, with their heads aligned with the robot base, holding the handle with their right hand (see figure 2). An adjustable strap was employed to hold the participants' elbow at the same height as their shoulder and the robotic end-effector, and to compensate for the arm's

weight. The strap was fixed to a slider, to compensate for the gravity without exerting lateral forces on the arm.

The task was displayed on a vertical monitor, thus forth/back movements of the handle were displayed as up/down movements of the cursor.

The robot control was implemented in C++ language, using Qt and Franka Control Interface libraries. It ran on Ubuntu 16.04 with a real-time kernel. The reaching task was implemented in C# language in the Unity 3D environment and ran on Windows 10. The robot control exchanged data with the task game through UDP communication. Data relative to the robot status (position, orientation, etc.) were employed for both task visualization and subsequent data analysis.

G. Data Analysis

Handle trajectories were considered excluding the first and last samples, which correspond either to unsteady starting or to fine adjustment at the end. For each movement, we evaluated the handpath error as the deviation from a straight line connecting the starting position to the target. This index was assessed both as the mean absolute error (MAE), and as the relative deviation to the left or the right of the straight path (signed mean error ME, with positive values indicating deviations to the right and negative to the left) [21]. In order to exclude the large variability given by the initial and final adjustments, the indices and the mean trajectories were assessed after having excluded the initial and final parts of the movement (i.e. calculated from the 8% to the 92% of the total path).

For each position, both trajectories and deviation indices were averaged across participants. We evaluated the global average deviation (MAE) over the three repetitions, but we considered only the last repetition for the data analysis to exclude the familiarization phase.

To better understand how the different starting positions in the workspace affect the lateral deviations, we fitted the mean error index (ME) across the 15 positions with three alternative polynomial functions, of the first, second and third-order respectively:

$$y(x) = p_3 x^3 + p_2 x^2 + p_1 x + p_0 \,, \tag{5}$$

where either p_3 or p_3 and p_2 are null in the case of second and first-order polynomials, respectively. p_0 value corresponds to the average amount of deviation at $x = 0$, i.e., on the workspace middle line. Fitting results were evaluated in terms of the goodness of fitting (adjusted R^2) and p_0 value. Additionally, we measured the interaction forces exerted by participants during the task, for each workspace position.

III. Results

Fig. 3 shows the mean absolute handpath error for the two configurations across the 15 positions of the workspace and over the three repetitions. It is visible how the amount of perturbation provided by the robot in the first repetition decreased and settled already during the second repetition. On average (mean value across all positions) the deviation

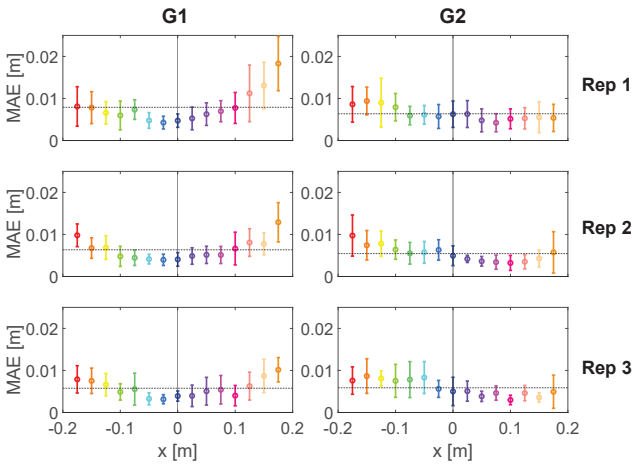

Fig. 3. Mean Absolute Error (deviation from the straight line), for the three repetitions (Rep 1,2,3) with the robot configurations G1 and G2, respectively. MAE value is reported as the mean and standard deviation across participants and trials, for each of the 15 positions of the workspace. Each repetition is composed of 30 trials, two for each position. The dashed line represents the average value across the workspace.

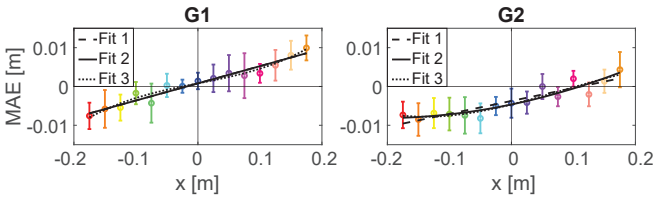

Fig. 4. Average signed deviation from the straight line (mean error) is reported as mean and standard deviation across eight participants and two trials per participant, for each of the 15 positions of the workspace. Dashed, solid and dotted black lines represent respectively the first, second and third-order polynomial fitting of the mean values. All these data refer to the last repetition only.

decreased by 19% and 14% between the first and second repetition, for configuration G1 and G2, respectively; it then slightly oscillated (decreases by 9% in G1 and increased by 7% in G2) between the second and third repetition, reaching in the last one the average values of 5.8 mm $\pm$ 2.1 mm for G1 and 5.9 mm $\pm$ 1.9 mm for G2. Besides decreasing over time, the deviation presented higher values at the boundaries rather than in the workspace centre, particularly for G1. Considering this result, for the other metrics we reported only the results relative to the last repetition.

Figure 4 shows the signed deviations and their fitting for the two configurations, considering first, second and third-order polynomials. The best fittings for configuration G1 and G2 were respectively the third-order and second-order polynomial, with adjusted R^2 values equal to 0.96 and 0.85. The magnitude of the deviation from the straight line in the workspace centre, i.e., p_0 value, for configuration G2 resulted bigger (4.6 mm) than for configuration G1 (0.8 mm).

The main difference between the two setups is the shape of the fitting, which represents the variation of the force field across the workspace. Configuration G1 resulted best fitted with a third-order polynomial: it showed almost null deviations in the central positions and higher deviations

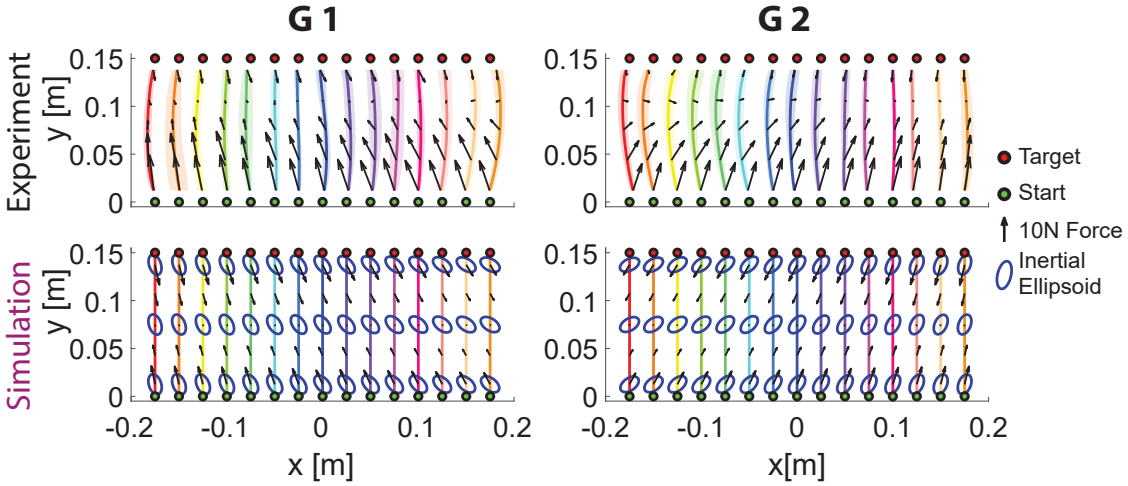

Fig. 5. Performance with configuration G1 and G2 in simulation and experiment. Motion trajectories for the 15 positions are represented as mean (solid line) and standard deviation (shadow) across participants and trials. Green and red dots represent the starting points and the targets, respectively. Estimated inertial forces and ellipsoids are reported for the simulation. Measured interaction forces are shown for the experiment. All the experimental data refer to the last repetition only.

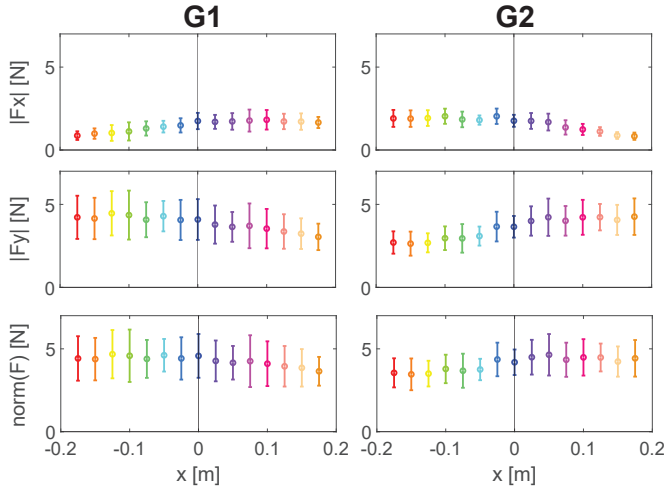

Fig. 6. Interaction forces for configuration G1 and G2 expressed as absolute value along x, absolute value along y and norm. Each value is represented as mean and standard deviation for each workspace position. These data refer to the last repetition only.

at the workspace boundaries. Interestingly, those boundary deviations were symmetric with respect to the side, i.e., on the right side people tended to deviate to the right and on the left side they tended to deviate to the left. Conversely, configuration G2 showed a less symmetric behaviour, which led to negative deviations (toward the left) in most of the workspace, except for the right boundary, where the deviations oscillate around zero. The amount of deviation is higher on the left boundary and decreases according to a second-order trend heading to the right boundaries.

Figure 5 shows the results related to the simulations and the experiments in terms of motion paths, interaction forces and inertia across the workspace. At intermediate points of each simulated straight path, we depicted the generalized inertial ellipses and inertial forces estimated by the simulations.

The first evident and predictable result is the symmetry of the inertial contribution between the two mirrored configurations G1 and G2. Ellipses are tilted in the same way for a given robot configuration, i.e., counterclockwise with respect to the vertical axis for G1 and clockwise for G2. As expected, the ellipses' orientation is configuration dependent, being less tilted on the left boundary for G1 and on the right one for G2.

For the experimental data, we showed the average trajectories performed by participants for all 15 positions, and the average interaction forces exerted by participants along five intermediate points of each trajectory. On average, the interaction forces were comparable with the simulated ones in terms of direction, even though they presented slightly higher magnitude at the beginning and lower at the end of the trajectory, probably due to unmodelled friction contribution. In fact, differently from the simulations, in which the interaction forces are symmetric with respect to the middle point of the path, the experimental forces were greater in the first half of the trajectory and lower in the second part.

Interaction forces are also reported more in detail in figure 6, in terms of average values of the norm, and mean absolute values along the x and y axes separately, averaged across participants for each workspace position. The norm of the force resulted to be lower than 5N for both G1 and G2. However, while the norm remains roughly constant across the workspace, this is not true when we look at the separate contributions along the x and y axes: the y contribution resulted higher where the ellipsoids are vertically aligned (left boundary for G1 and right boundary for G2), while it decreased on the other side, where the x contribution increased in the opposite way, accordingly to the ellipses' orientation.

IV. Discussion

In the present work, we assessed the suitability of a 7 DoFs robotic manipulator as a transparent haptic interface for motor neuroscience studies. In particular, we tested two

robot planar configurations, named G1 and G2, which differ in the location of the robot's elbow (on the left or right side of the workspace) while controlling the robot with impedance control, compensating for the gravity, Coriolis and centrifugal, and joint friction contributions.

First, we estimated the inertial ellipses and simulated inertial forces across space for human-like reaching movements. Then, we assessed the amount of perturbation provided by the robot to the human motion in terms of the deviation from the straight path and interaction forces.

After the first task repetition, the global amount of deviation decreased and settled for both configurations. This means that the perturbation due to the presence of the robot decreased after 2 minutes of interaction with the device, leading to an average deviation lower than 6 mm. It is worth noting that this value represents the average across all 15 positions spanning over the workspace but, especially for G1, the perturbation showed lower values in the central positions compared to the boundaries.

This trend is confirmed by the highest goodness of fitting of the signed handpath error with a third-order polynomial, for G1. Moreover, it showed concordance between path deviations and workspace sides, deviating to the left in the left workspace and to the right in the right one. This is an interesting aspect worth discussing.

Indeed, by looking at the simulation and experimental results, it is evident how the presence of the human arm, with its own posture and inertia, affected the outcomes. The estimated inertial forces are specular in the two configurations and symmetrical with respect to the middle point of the trajectory. However, probably due to the static friction contribution, the interaction forces detected in the real scenario were higher at the beginning of the movement and lower at the end. The horizontal (x) force contribution in G2 resulted to be more prominent in the left and the central part of the workspace, where also a negative (to the left) deviation was present. In this part of the workspace, both the robotic and human arms are in their most extended posture. On the contrary, in G1 the extension of the human arm corresponds to the flexed configuration of the robotic arm and vice versa. This is probably the reason why G1 led to deviations symmetrical with respect to the centre of the workspace.

As regards the deviation amount, a slightly reduced workspace, which excludes one or two boundary points, allows the planar configuration G1 to provide very little perturbation in terms of trajectory deviations, so that it can be considered a good configuration for experiments on human subjects. This is not true in the G2 case where, even with a workspace restriction, the robot affects the arm's movement, with residual deviations arranged in an asymmetrical way with respect to the centre of the workspace.

The presented results show that a general-purpose collaborative manipulator could be used in motor neuroscience studies to provide carefully controlled perturbations and observe how the human motor system reacts to them, without introducing unintended and noisy motor interference. This could pave the way for future works that may extend the investigation of human movements to more complex 3D tasks.

REFERENCES

[1] E. Burdet, R. Osu, D. W. Franklin, T. E. Milner, and M. Kawato, "The central nervous system stabilizes unstable dynamics by learning optimal impedance," *Nature*, vol. 414, no. 6862, pp. 446–449, 2001.

[2] D. W. Franklin, R. Osu, E. Burdet, M. Kawato, and T. E. Milner, "Adaptation to stable and unstable dynamics achieved by combined impedance control and inverse dynamics model," *Journal of neurophysiology*, vol. 90, no. 5, pp. 3270–3282, 2003.

[3] J. B. Heald, J. N. Ingram, J. R. Flanagan, and D. M. Wolpert, "Multiple motor memories are learned to control different points on a tool," *Nature human behaviour*, vol. 2, no. 4, pp. 300–311, 2018.

[4] T. Brashers-Krug, R. Shadmehr, and E. Bizzi, "Consolidation in human motor memory," *Nature*, vol. 382, no. 6588, pp. 252–255, 1996.

[5] R. Shadmehr and F. A. Mussa-Ivaldi, "Adaptive representation of dynamics during learning of a motor task," *Journal of neuroscience*, vol. 14, no. 5, pp. 3208–3224, 1994.

[6] R. Osu, E. Burdet, D. W. Franklin, T. E. Milner, and M. Kawato, "Different mechanisms involved in adaptation to stable and unstable dynamics," *Journal of Neurophysiology*, 2003.

[7] F. A. Mussa-Ivaldi, N. Hogan, and E. Bizzi, "Neural, mechanical, and geometric factors subserving arm posture in humans," *Journal of neuroscience*, vol. 5, no. 10, pp. 2732–2743, 1985.

[8] D. W. Franklin, G. Liaw, T. E. Milner, R. Osu, E. Burdet, and M. Kawato, "Endpoint stiffness of the arm is directionally tuned to instability in the environment," *Journal of Neuroscience*, vol. 27, no. 29, pp. 7705–7716, 2007.

[9] B. T. Volpe *et al.*, "Robotics and other devices in the treatment of patients recovering from stroke," *Current neurology and neuroscience reports*, vol. 5, no. 6, p. 465, 2005.

[10] V. Klamroth-Marganska, J. Blanco, K. Campen, A. Curt, V. Dietz, T. Ettlin, M. Felder, B. Fellinghauer, M. Guidali, A. Kollmar *et al.*, "Three-dimensional, task-specific robot therapy of the arm after stroke: a multicentre, parallel-group randomised trial," *The Lancet Neurology*, vol. 13, no. 2, pp. 159–166, 2014.

[11] G. B. Prange, M. Jannink, C. Groothuis-Oudshoorn, H. J. Hermens, and M. J. IJzerman, "Systematic review of the effect of robot-aided therapy on recovery of the hemiparetic arm after stroke," 2009.

[12] D. M. Wolpert, J. Diedrichsen, and J. R. Flanagan, "Principles of sensorimotor learning," *Nature reviews neuroscience*, vol. 12, no. 12, pp. 739–751, 2011.

[13] L. Zollo, L. Rossini, M. Bravi, G. Magrone, S. Sterzi, and E. Guglielmelli, "Quantitative evaluation of upper-limb motor control in robot-aided rehabilitation," *Medical & biological engineering & computing*, vol. 49, pp. 1131–1144, 2011.

[14] G. Rosati, R. Secoli, D. Zanotto, A. Rossi, and G. Boschetti, "Planar robotic systems for upper-limb post-stroke rehabilitation," vol. 48630, pp. 115–124, 2008.

[15] H. I. Krebs, N. Hogan, M. L. Aisen, and B. T. Volpe, "Robot-aided neurorehabilitation," *IEEE transactions on rehabilitation engineering*, vol. 6, no. 1, pp. 75–87, 1998.

[16] L. Zollo, D. Accoto, F. Torchiani, D. Formica, and E. Guglielmelli, "Design of a planar robotic machine for neuro-rehabilitation," pp. 2031–2036, 2008.

[17] M. Pinardi, L. Raiano, D. Formica, and G. Di Pino, "Altered proprioceptive feedback influences movement kinematics in a lifting task," *2020 42nd Annual International Conference of the IEEE Engineering in Medicine & Biology Society (EMBC)*, pp. 3232–3235, 2020.

[18] O. Khatib, "Inertial properties in robotic manipulation: An object-level framework," *The international journal of robotics research*, vol. 14, no. 1, pp. 19–36, 1995.

[19] C. A. Klein and K.-B. Kee, "The nature of drift in pseudoinverse control of kinematically redundant manipulators," *IEEE Transactions on robotics and automation*, vol. 5, no. 2, pp. 231–234, 1989.

[20] R. C. Oldfield, "The assessment and analysis of handedness: The edinburgh inventory," *Neuropsychologia*, vol. 9, no. 1, pp. 97–113, 1971.

[21] D. W. Franklin, E. Burdet, K. P. Tee, R. Osu, C.-M. Chew, T. E. Milner, and M. Kawato, "Cns learns stable, accurate, and efficient movements using a simple algorithm," *Journal of neuroscience*, vol. 28, no. 44, pp. 11 165–11 173, 2008.